



1    **Recent decrease in summer precipitation over the Iberian Peninsula**  
2    **closely links to reduction of local moisture recycling**

3    Yubo Liu<sup>1,2</sup>, Monica Garcia<sup>3</sup>, Chi Zhang<sup>1,4</sup>, Qihong Tang<sup>1,2\*</sup>

4

5    <sup>1</sup>Key Laboratory of Water Cycle and Related Land Surface Processes, Institute of Geographic

6    Sciences and Natural Resources Research, Chinese Academy of Sciences, Beijing, China

7    <sup>2</sup>University of Chinese Academy of Sciences, Beijing, China

8    <sup>3</sup>Department of Environmental Engineering, Technical University of Denmark, Lyngby, 2800,

9    Denmark

10    <sup>4</sup>Key Laboratory of Land Surface Pattern and Simulation, Institute of Geographic Sciences and

11    Natural Resources Research, Chinese Academy of Sciences, Beijing, China

12

13    **\*Correspondence:** Qihong Tang (tangqh@igsnr.ac.cn)

14



## 15 **Abstract**

16 The inherently dry summer climate of the Iberian Peninsula (IP) is undergoing drought  
17 exacerbated by more intense warming and reduced precipitation. Although many  
18 studies have studied changes in summer climate factors, it is still unclear how the  
19 changes in moisture contribution from the source lead to the decrease in summer  
20 precipitation. This study investigates the differences in the IP precipitationshed between  
21 1980-1997 and 1998-2019 using the Water Accounting Model-2layers with ERA5 data,  
22 and assesses the role of local recycling and external moisture in reducing summer  
23 precipitation. Our findings indicate that the moisture contributions from the local IP,  
24 and from the west and the east of the precipitationshed contributed 1.7, 3.6 and 1.1 mm  
25  $\text{mon}^{-1}$  less precipitation after 1997 than before 1997, accounting for 26 %, 57 % and  
26 17 % of the main source supply reduction, respectively. The significant downward trend  
27 of the IP local recycling closely links to the disappearance of the wet years after 1997  
28 as well as the decrease of local contribution in the dry years. Moreover, the feedback  
29 between the weakened local moisture recycling and the drier land surface can  
30 exacerbate the local moisture scarcity and summer drought.  
31



## 32 **1. Introduction**

33       The Iberian Peninsula (IP) is located in the Mediterranean area, which is among  
34 the global “hotspots” of climate change. The IP precipitation is characterized by the  
35 diverse climatic regimes and high spatial variability as a consequence of its geographic  
36 position between the Atlantic Ocean and the Mediterranean Sea and its orographic  
37 configuration. In responding to climate change with frequent heatwaves and above-  
38 average warming, the IP is experiencing widespread decreases in precipitation,  
39 especially in summer (Brogi et al., 2019; Cramer et al., 2018; Rajczak and Schär, 2017).  
40 This reduction in summer precipitation is a major driver of water resource depletion  
41 and the evolution of drought (Lopez-Bustins and Lemus-Canovas, 2020; Páscoa et al.,  
42 2021; Teuling et al., 2013). To clarify the reason for the decrease in summer  
43 precipitation, it is necessary to explain the changes in moisture contribution from the  
44 source, such as local recycling and external sources.

45       Analysis of source supply and transportation in the hydrological cycle has become  
46 one efficient way to understand well regional precipitation. With the introduction of the  
47 concept of precipitationshed (Keys et al., 2014; Keys P. W. et al., 2011), which better  
48 reveals the contribution from upwind evaporation sources to precipitation in downwind  
49 sink region, it is more scientific and systematic to explain the precipitation variations  
50 by using the fluctuations of moisture contribution as a precursor. Given the importance  
51 of studying the source of precipitation, that is, precipitationshed, a variety of methods  
52 have been developed and adopted, including physical isotope analysis (Bonne et al.,



53 2014), and numerical analytical models, either online methods running in parallel with  
54 climate models (Damián and Gonzalo, 2018; Stohl and James, 2004, 2005), or offline  
55 “posteriori models” (van der Ent and Savenije, 2011; van der Ent et al., 2010; van der  
56 Ent et al., 2013). Although the mechanisms of these studies are different, they all  
57 emphasize that the constantly changing source-sink relationship of atmospheric  
58 moisture is an essential part of climate change research as global change continues.

59 Gimeno et al. (2010) comprehensively investigated the atmospheric moisture  
60 sources of the IP precipitation at different scales, and identified the tropical–subtropical  
61 North Atlantic corridor, the surrounding Mediterranean Sea and the local IP as the  
62 important moisture regions. The high precipitation in the cold season is mainly  
63 dominated by westerly wind regimes. The mid-latitude atmospheric dynamics, such as  
64 the baroclinic synoptic-scale perturbations from the Atlantic and the polar jet stream,  
65 as well as the high moisture supply from an Atlantic “tropospheric river” seem to be  
66 responsible for the abundant precipitation during the cold season (Cortesi et al., 2013;  
67 Ulbrich et al., 2015; Zhu and Newell, 1998). Compared to the rainy winter, the summer  
68 with very low precipitation receives less attention. The subtropical location under the  
69 descending air extending from the North Atlantic subtropical high controls low summer  
70 precipitation over the IP, and local convective events increase the importance of local  
71 recycling during summer (Serrano et al., 1999). Accordingly, the summer IP  
72 precipitation, a significant proportion of which is taken up by the local recycled water  
73 vapor, is completely different from the precipitation in winter that is dominated by the



74 moisture transported over long distances from external sources.

75 In recent decades, the increasing severity of summer drought in the IP, which is  
76 closely related to precipitation variations, has attracted more attention. Several  
77 mechanisms, including soil-atmosphere interactions (Boé and Terray, 2014), cloud  
78 processes (Lenderink et al., 2007; Tang et al., 2012) and large-scale circulation changes  
79 (Boé et al., 2009; Brogli et al., 2019; Kröner et al., 2017), have been found to be  
80 potentially important for this complex summer climate change, which also appear to  
81 have an impact on precipitation reduction. However, there is still a lack of  
82 understanding of such summer precipitation decline in terms of changes in the moisture  
83 contribution from the source. Therefore, tracing the precipitation shed of the IP and  
84 quantifying the moisture contributions can provide us with a new perspective to analyze  
85 the changes in IP precipitation. This study aims to evaluate the moisture contribution  
86 of local recycling and external sources to the reduction of IP summer precipitation.

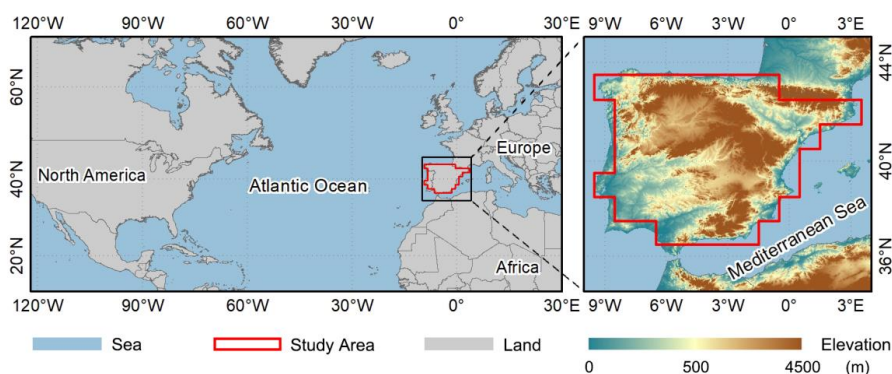
## 87 **2. Study Area, Data and Methods**

### 88 **2.1 Study area**

89 The IP is located in southwestern Europe at midlatitudes of the northern  
90 hemisphere. It covers Portugal and the mainland of Spain. The geographic location of  
91 IP is shown in Fig. 1(a) (36°N-44°N, 10°W-3°E) in a transition zone between  
92 midlatitude and subtropical atmospheric circulation regimes. It has a complex  
93 topography, surrounded by the Atlantic Ocean and Mediterranean Sea, and high in the



94 middle and northeast. The topographic and coastal processes affect water vapor  
95 transport, forming a spatial precipitation gradient from northwest to southeast.  
96 Extracted from the land-sea mask provided by European Centre for Medium-range  
97 Weather Forecasts (ECMWF), the red outline area composed of multiple single 1×1  
98 degree grids is our study area of IP.



99  
100 **Figure 1** Map of the IP (the area within the closure of the red line) on a grid of 1°×1° as the target  
101 region.

## 102 103 2.2 Data

104 The newest reanalysis data held in ECMWF data archive, ERA5 dataset  
105 downloaded from the Copernicus Climate Change Service (C3S) Climate Data Store  
106 (CDS) is used in this study (Hersbach et al., 2020). The variables include surface  
107 pressure, precipitation, evaporation, total column water, and vertical integrated  
108 eastward and northward atmospheric water fluxes (including cloud liquid water flux,  
109 cloud frozen water flux and water vapor flux) on single level, as well as the horizontal



110 U/V components of wind fields and specific humidity at the lowest 23<sup>rd</sup> pressure levels  
111 (200-1000hPa). The time resolution and spatial resolution selected for these data are 1  
112 hour and 1×1 degree, respectively. This dataset covers the period from 1980 to 2019.  
113 Compared to the old version reanalysis data (e.g., ERA-Interim or ERA-40), ERA5  
114 combines vast amounts of historical observations into global estimates using more  
115 advanced modelling and data assimilation systems (Hersbach et al., 2020).

116 To avoid the uncertainty of ERA5 precipitation as a global forecast data, its  
117 reliability in the IP needs to be verified. Therefore, an observational gridded dataset  
118 generated from a dense network of stations over the IP, named Iberia01 (Herrera et al.,  
119 2019), is used to verify the accuracy of ERA5 precipitation data. Iberia01 provides the  
120 daily precipitation for the period of 1971-2015 at 0.1×0.1 degree.

## 121 2.3 Model and methods

### 122 2.3.1 Water Accounting Model-2layers

123 Water Accounting Model-2layers (WAM-2layers) is an offline Eulerian method  
124 tracking the moisture cycle forwards or backwards that quantifies the source-sink  
125 relations (van der Ent et al., 2013; van der Ent et al., 2014). Its backward algorithm was  
126 used in this study to trace the precipitationshed of the IP. The model of WAM-2layers  
127 is an updated version of the original WAM. The water vapor balance equation in the  
128 WAM-2layers algorithm maintains the premise that the atmosphere is well mixed, but  
129 compared with the previous model, it takes the stratification of the atmosphere into



130 consideration. Thus, when the algorithm is applied to a specific region, the calculation  
131 is as follows,

$$132 \quad \frac{\partial W_{l,r}}{\partial t} + \frac{\partial(W_{l,r}u)}{\partial x} + \frac{\partial(W_{l,r}v)}{\partial y} = E_{l,r} - P_{l,r} \pm F_{v,r} + \alpha_{l,r} \quad (1)$$

133 where  $W$  is the atmospheric moisture storage, or namely, precipitable water;  $t$  is time;  $u$   
134 and  $v$  are the wind components in  $x$  (zonal) and  $y$  (meridional) direction, respectively;  
135  $E$  is evaporation;  $P$  is precipitation;  $F_V$  is the vertical moisture transport between the  
136 bottom and top layer;  $\alpha$  is a residual term; the subscript  $l$  represents the portion in layer  
137  $l$  (either the bottom layer or the top layer), and the subscript  $r$  represents the tagged  
138 portion provided by the source region.

139 Based on the assumption of a well-mixed atmosphere (Burde, 2010; Goessling and  
140 Reick, 2013), the moisture contribution, that is, the tagged evaporation  $E_r$ , can be  
141 calculated considering that the ratio of tagged to total atmospheric water storage is equal  
142 to the ratio of tagged to total evaporation, as shown in Eq. (2). Considering the proposed  
143 retention time of atmospheric moisture is about 1 week to 10 days (Numaguti, 1999),  
144 we set the backtracking time as 1 month for summer precipitation to make sure that  
145 more than 90 % of the precipitation can be redistributed to the surface.

$$146 \quad E_r(t, x, y) = \frac{W_r(t, x, y)}{W(t, x, y)} \times E(t, x, y) \quad (2)$$

147 The main moisture source supplying IP summer precipitation, that is, 90<sup>th</sup> percentile  
148 precipitationshed in this study, is divided into subregions to evaluate the role of the  
149 contribution from each area, such as local recycling and external advection moisture.





150 For each of the partitioned source region ( $A$ ), the proportion of the moisture  
 151 contribution from all grids covered by it to the total contribution from the main source  
 152 region ( $MS$ ) is the contribution ratio ( $CR$ ), which is calculated as the following Eq. (3).  
 153 The precipitation recycling ratio of the IP can be substituted with IP local contribution  
 154 ratio  $CR_{IP}$ .

$$155 \quad CR_A = \frac{\sum E_r(t, x, y|A)}{\sum E_r(t, x, y|MS)} \times 100\% \quad (3)$$

### 156 2.3.2 Significance test

157 The slope significance of trend fitting and the significance of the difference in the  
 158 means are tested using Student t-test in this study. Additionally, the mutation analysis  
 159 for detecting significant mutation in precipitation series is the sliding t-test,

$$160 \quad T = \frac{\frac{1}{n_1} \sum_{t=1}^{n_1} x - \frac{1}{n_2} \sum_{t=n_1+1}^{n_1+n_2} x}{\frac{(n_1-1)S_1^2 + (n_2-1)S_2^2}{n_1+n_2-2} \sqrt{\frac{1}{n_1} + \frac{1}{n_2}}} \quad (4)$$

161 where  $x$  is the precipitation series to be tested,  $n_1$  and  $n_2$  are step lengths set for two  
 162 sequences before and after the moving point, and  $S_1^2$  and  $S_2^2$  are the variances of the two  
 163 sequences which can be calculated as following.

$$164 \quad S_1^2 = \frac{1}{n_1-1} \sum_{t=1}^{n_1} \left( x - \frac{1}{n_1} \sum_{t=1}^{n_1} x \right)^2 \quad (5)$$

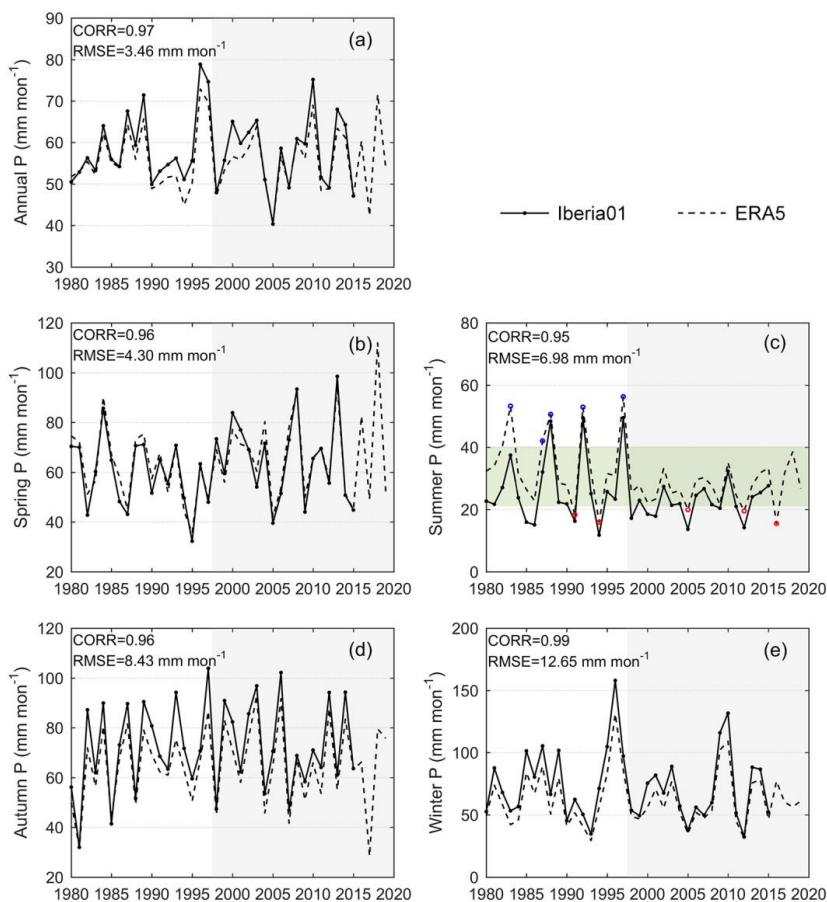
$$165 \quad S_2^2 = \frac{1}{n_2-1} \sum_{t=n_1+1}^{n_1+n_2} \left( x - \frac{1}{n_2} \sum_{t=n_1+1}^{n_1+n_2} x \right)^2 \quad (6)$$



## 166 **3. Results**

### 167 3.1 Evaluation and variation of precipitation data

168 The precipitation time series of ERA5 and Iberia01 data are shown in Fig. 2. The  
169 fluctuations and variations of ERA5 precipitation data are in good agreement with the  
170 observed data on both annual and seasonal scales, together with all correlation  
171 coefficients higher than 0.95. The average annual precipitation over the IP is about  
172 55.66 mm mon<sup>-1</sup> from ERA5 and 58.07 mm mon<sup>-1</sup> from Iberia01, respectively.  
173 Compared with the observed data, the reanalysis data slightly underestimates the IP  
174 precipitation with the root mean square error (RMSE) of 3.46 mm mon<sup>-1</sup> on the annual  
175 scale. The comparison of seasonal precipitation shows that ERA5 is lower than the  
176 observed Iberia01 value in the rainy seasons (both winter and autumn), but higher in  
177 the dry summer. The RMSE between the two datasets of seasonal precipitation is in the  
178 range of 4.30-12.65 mm mon<sup>-1</sup>. Since Iberia01 data is the grid data interpolated from  
179 observation site data (Herrera et al., 2019), some of the deviations between the ERA5  
180 and Iberia01 precipitation can be partially affected by the interpolation process rather  
181 than solely the result of the error generated by the reanalysis process. In general, ERA5  
182 precipitation data shows the characteristics of IP precipitation reasonably well and thus  
183 is suitable for studying the changes.



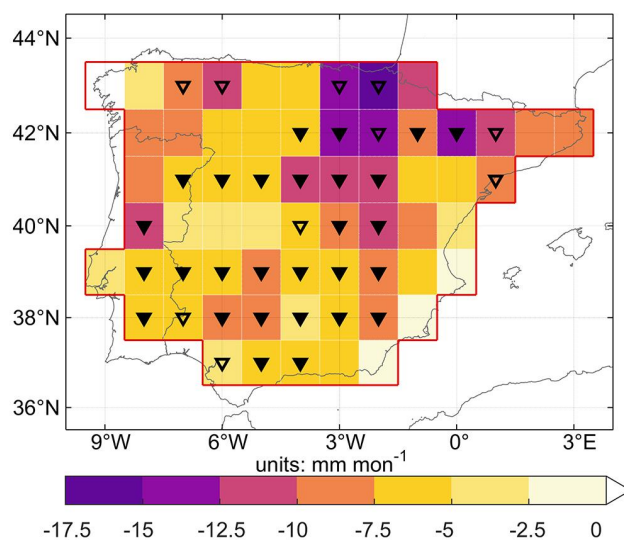
184

185 **Figure 2** Variations of IP annual precipitation (a), spring (March, April and May, b),  
186 July and August, c), autumn (September, October and November, d) and winter (December, January  
187 and February, e) during 1980-2019. The green shading covers the interval of one standard deviation  
188 of summer precipitation. The years with summer ERA5 precipitation exceeding the range of the  
189 green shading interval are circled in blue and red.

190 Only in summer, the mutation analysis of the two sets of precipitation data,  
191 Iberia01 and ERA5, both show statistically significant changes in 1997. Accordingly,



192 the entire 40-year period is divided into two periods, 1980-1997 and 1998-2019, to  
193 compare the difference in summer precipitation between the two periods. The average  
194 summer precipitation is 34.89 and 27.17 mm mon<sup>-1</sup> before and after 1997, respectively.  
195 Compared with 1980-1997, the average summer precipitation during 1998-2019  
196 decreases by 7.72 mm (22.13 %) in the whole study area. On the grid scale, almost all  
197 grids have less precipitation after 1997, and more than half of all grids show the  
198 statistically significant reductions (Fig. 3). However, this change is unevenly distributed  
199 in space, as shown by the greater reduction in the grids on the northeastern IP that can  
200 even exceed 10 mm mon<sup>-1</sup>.



201  
202 **Figure 3** The difference of average summer precipitation over the IP between 1998-2019 and 1980-  
203 1997 (average of 1998-2019 minus average of 1980-1997). The triangles indicate the differences  
204 are significant at 0.05 (solid) and 0.1 (hollow) level.



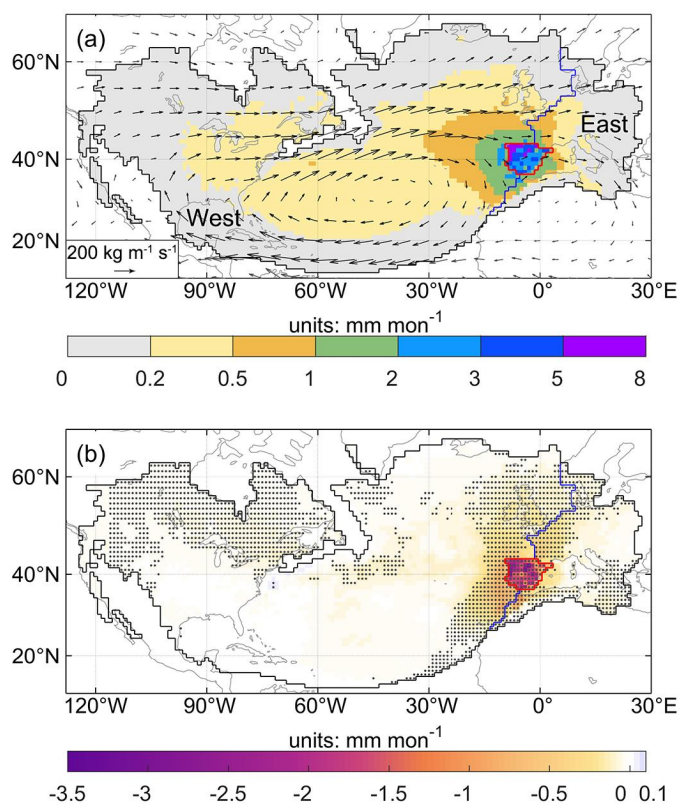
205 For summer precipitation, the dry years (1991, 1994, 2005, 2012 and 2016) and  
206 the wet years (1983 1987 1988 1992 and 1997) are selected, which are circled in Fig.  
207 2(c). A wet year is defined as the year in which the precipitation is more than one  
208 standard deviation above the average precipitation, and similarly, the precipitation in a  
209 dry year is lower than a standard deviation range. Accordingly, the division of time  
210 period also applies to the precipitation series of the dry and wet years. It is specifically  
211 observed that the dry years are separated, with the average precipitation of 17.15 and  
212 18.34 mm mon<sup>-1</sup> before and after 1997, whereas wet years occur before 1997 with an  
213 average of 51.03 mm mon<sup>-1</sup> but disappear after 1997.

### 214 3.2 Changes in summer precipitation shed and regional contributions

215 From 1980 to 2019, an average of 28.53 mm mon<sup>-1</sup> precipitation has been tracked  
216 by the global surface, exceeding 93 % of IP summer precipitation with an average of  
217 30.64 mm mon<sup>-1</sup>. The climatology of the moisture contribution during the 40 years is  
218 shown in Fig. 4 (a). The moisture contribution to IP generally decreases as its distance  
219 to IP increases. Although the precipitation shed of IP summer precipitation is global in  
220 scope, the contribution of the area far away is negligible to be considered. Therefore,  
221 the 90<sup>th</sup> precipitation shed enclosed by the black line in Fig. 4 is given full attention as  
222 the main moisture source region in the following text. The main moisture source of the  
223 IP covers not only the local grids in the study region, but also several of non-local land  
224 and oceanic areas. Due to the dominance of the westerlies in tropical–subtropical North



225 Atlantic corridor (Gimeno et al., 2010), as shown by the circulation in the Fig. 4(a),  
226 most of the non-local source grids are located in the North American land and North  
227 Atlantic Ocean to the west of the study area. The other source grids are located east of  
228 North Atlantic Ocean and the IP, which is the downwind zone for water vapor transport,  
229 covering Western Europe and the Mediterranean. Hence, the main moisture sources are  
230 divided into the three partial regions of the local IP, the west and the east by the  
231 boundary of the study area and the eastern boundary of the Atlantic Ocean (red and blue  
232 lines in Fig. 4), and the contribution of each region to IP precipitation can be quantified  
233 and compared.



234



235 **Figure 4 (a)** Climatological 90<sup>th</sup> precipitationshed of the IP sink region and moisture contribution  
236 to IP summer precipitation from 1980 to 2019. The black outlines show the 90<sup>th</sup> precipitationshed  
237 boundary during the 40 years. The vectors represent the climatological monthly water vapor flux.  
238 The red line encloses the study area, and the blue line divides the precipitationshed excluding the IP  
239 into the west (left area) and the east (right area) regions. (b) Difference in moisture contribution in  
240 the 90<sup>th</sup> precipitationshed between 1980-1997 and 1998-2019 (average of 1998-2019 minus average  
241 of 1980-1997). The dots indicate 0.1 significance of the difference.

242 Affected by the transport distance, the grids with high contribution are located in  
243 and around the target IP region, with the maximum values for grids in the northwest  
244 corner of the IP. The local IP contributes 3.46 mm mon<sup>-1</sup> average summer precipitation,  
245 with the precipitation recycling ratio of around 13.26 % during the 40 years. The west,  
246 as the largest sub-region of the precipitationshed, contributes the most summer  
247 precipitation of 19.38 mm mon<sup>-1</sup> and occupies 76.06 % of the tracked precipitation  
248 averagely. While the east region, which is in an unfavorable downwind position in the  
249 summer circulation, provides only 2.81 mm mon<sup>-1</sup> summer precipitation, accounting  
250 for 10.68 %.

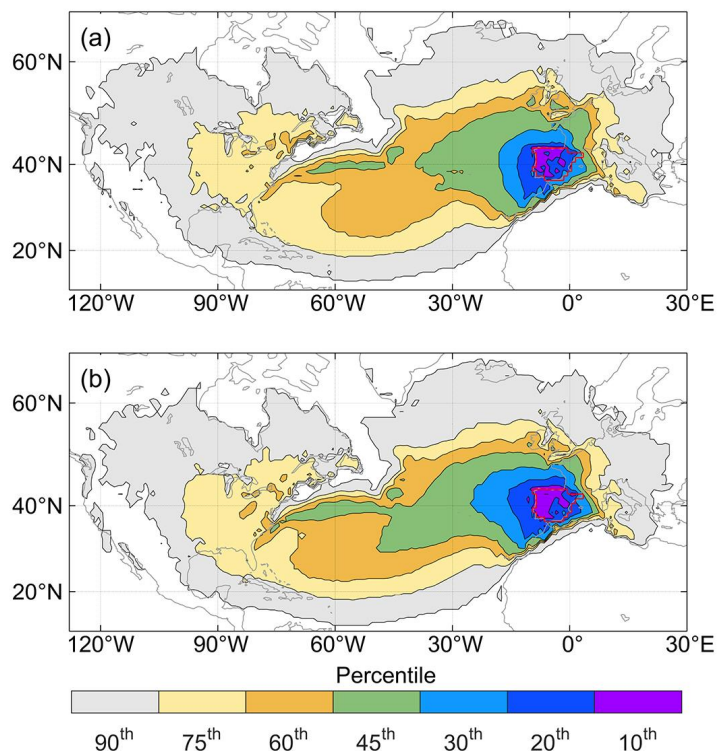
251 The difference in moisture contribution obtained from the 1998-2019 period minus  
252 the 1980-1997 period is shown in Fig. 4(b). Almost all grid contributions show a  
253 decrease after 1997. The grids with a large moisture contribution decline are mainly  
254 concentrated in the IP, with the maximum reduction exceeding an average of 3 mm  
255 mon<sup>-1</sup>. Compared with other non-local source grids, the grids with higher contributions



256 along the east coast of the North Atlantic near the IP also have a slight but significant  
257 reduction in contribution.

258 Due to the uneven distribution of grid contribution reduction in space, the area of  
259 different percentile precipitationsheds differs in the two periods. The areas with  
260 different colors in the distribution map of Fig. 5 represent the precipitationshed  
261 boundaries at different percentiles in the two periods. During 1998-2019, the  
262 precipitationshed boundary of each percentile extends westward in varying degrees  
263 compared with those before 1997. The top decile of the contribution is still in the  
264 western half of the IP. In the North Atlantic, the westward expansion of the western  
265 boundary of the precipitationsheds is conspicuous, especially the 45th and 60th  
266 percentile precipitationsheds shown in orange and green color in Fig. 5(a, b). This  
267 westward extension implies that the significant and substantial reduction in the  
268 contribution of the local grids and its surrounding grids results in a decrease in the  
269 proportion of these areas. Therefore, for the same percentile of the precipitationshed,  
270 only a smaller area concentrated by high-contribution grids is sufficient before 1997.  
271 However, a larger area is required for the same proportion after 1997.





272

273 **Figure 5** Different percentile precipitation sheds during the two periods 1980-1997 (a) and 1998-

274 2019 (b).

275 Figure 6(a) shows the quantified precipitation contributed by the local IP, the west

276 and the east regions. The negative slopes in Fig. 6(a) indicate that the summer

277 precipitation contributed by these three regions has a downward trend, especially

278 significant for the IP and the west with slopes of  $-0.59$  and  $-1.28 \text{ mm mon}^{-1} \text{ decade}^{-1}$ .

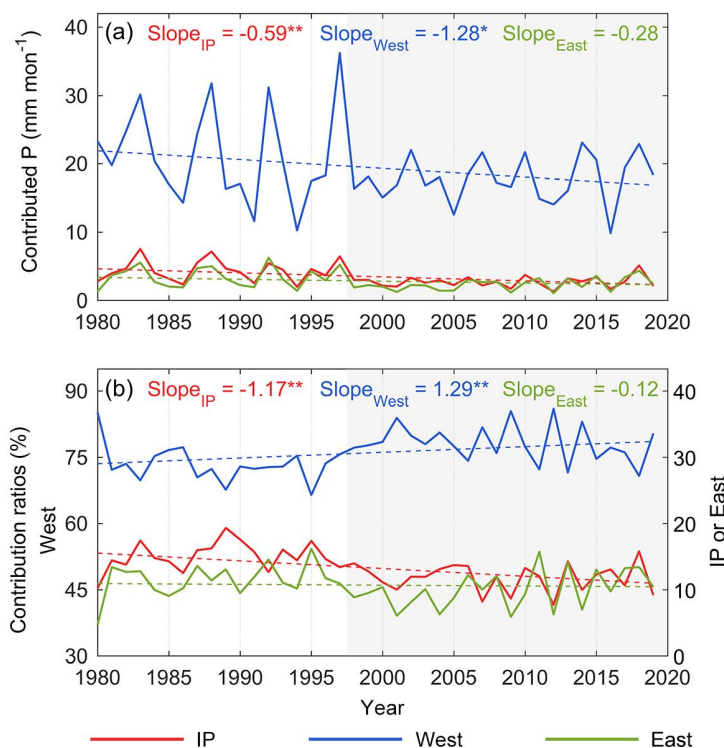
279 These decreasing trends cause a  $6.38 \text{ mm mon}^{-1}$  difference in precipitation from the

280 main source region in the two periods, which explain 82.64 % of the total reduction in

281 IP summer precipitation ( $7.72 \text{ mm mon}^{-1}$ ). In terms of the difference in the average



282 values of each region, the precipitation contributed by the local IP, the west and the east  
 283 significantly decreases from 4.38, 21.37 and 3.41 mm mon<sup>-1</sup> in 1980-1997 to 2.71,  
 284 17.76 and 2.32 mm mon<sup>-1</sup> in 1998-2019, respectively. 26.32 %, 56.53 % and 17.15 %  
 285 of the difference in main source supply between the two periods are due to the  
 286 contribution decline from the local IP, the west and the east, respectively.



287  
 288 **Figure 6** Variations of contributed precipitation (a, unit of the slope: mm mon<sup>-1</sup> decade<sup>-1</sup>) and  
 289 contribution ratios (c, unit of the slope: % decade<sup>-1</sup>) from the IP, the west and the east region during  
 290 1980-2019 summer. ‘\*\*\*’ and ‘\*\*’ represent 0.05 and 0.1 level significance of the trend.

291 The variation and trend of the contribution ratio of each region are shown in Fig.  
 292 6(b). The proportion of contributions from the local IP and the east shows a decreasing



293 trend throughout the 40 years with the slope of  $-1.17\% \text{ decade}^{-1}$  and  $-0.12\% \text{ decade}^{-1}$ ,  
294 which is consistent with the decreasing trends of their absolute contributions.  
295 Conversely, although the precipitation contributed by the west shows a decreasing trend,  
296 its proportion is significantly increasing and the slope is  $1.29\% \text{ decade}^{-1}$ . The average  
297 contribution ratios of the local IP and the east decrease from 15.05 % and 11.49 %  
298 before 1997 to 11.79 % and 10.02 % after 1997, while the ratio of the west increases  
299 from 73.46 % to 78.19 %.

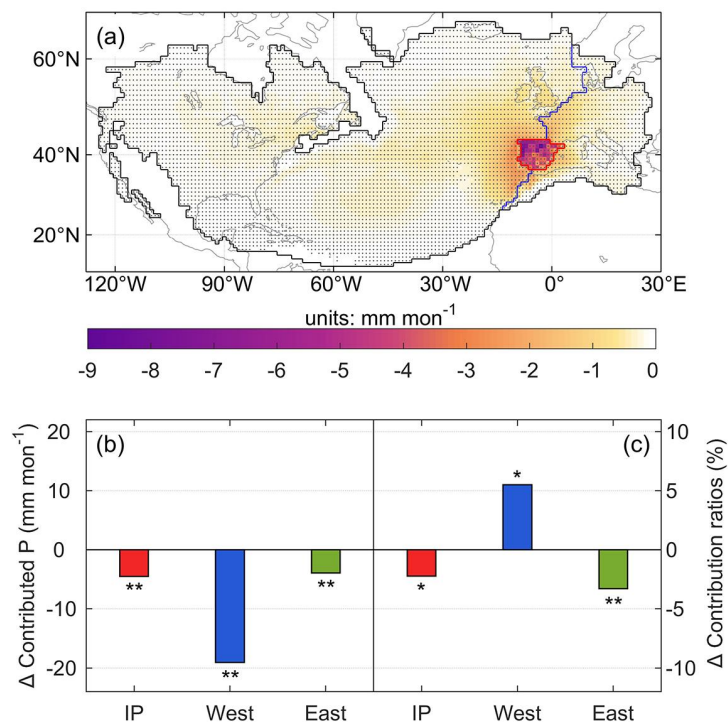
### 300 3.3 Differences in wet years and dry years

301 The dry years (1991, 1994, 2005, 2012 and 2016) and the wet years (1983 1987  
302 1988 1992 and 1997) are selected as described in section 3.1. Of the two divided periods,  
303 all the wet years only occur before 1997, while the dry years are distributed in both  
304 periods with no decrease in its average value. This represents that although the average  
305 summer precipitation after 1997 is reduced significantly compared with the previous  
306 period, there is no decrease in the valley value of the precipitation series. Thus, the  
307 disappearance of the wet years during 1998-2019 caused by the decrease of the  
308 precipitation series peaks directly reflects the recent decrease in IP summer  
309 precipitation.

310 During the entire 40 years, the difference in moisture contribution within the 90<sup>th</sup>  
311 precipitation shed of IP summer precipitation between wet and dry years is shown in  
312 Fig. 7(a). In the dry years, the significant reduction in the moisture contribution from



313 all grids in the main source region induces much lower precipitation than in the wet  
314 years. On the grid scale, the larger declines primarily happened in the local IP, and the  
315 grids with the largest drop, close to  $9 \text{ mm mon}^{-1}$ , are mainly concentrated in the west  
316 and north of the IP. In each source region, an average of 6.41, 30.74 and  $5.34 \text{ mm mon}^{-1}$   
317 of summer IP precipitation is provided from the local IP, the west and the east in the  
318 wet years, with 15.15 % recycling ratio, 72.19 % and 12.66 % contribution ratio. While  
319 in the dry years, the average precipitation contributed from each region is 1.92, 11.66  
320 and  $1.40 \text{ mm mon}^{-1}$ , accounting for 12.93 %, 77.70 % and 9.37 %, respectively. All  
321 three regions contribute more to summer precipitation in wet years than in dry years,  
322 and compared with dry years, the contribution ratios of the local IP and the east in wet  
323 years are also higher. The disappearance of wet years during 1998-2019 further  
324 motivates similar changes between the two periods. The decrease in the frequency of  
325 wet years with higher local recycling ratio and higher contribution ratio of the east leads  
326 to an increase in the proportion of the summer precipitation originating from the  
327 remaining other region, namely the west, during the same period.



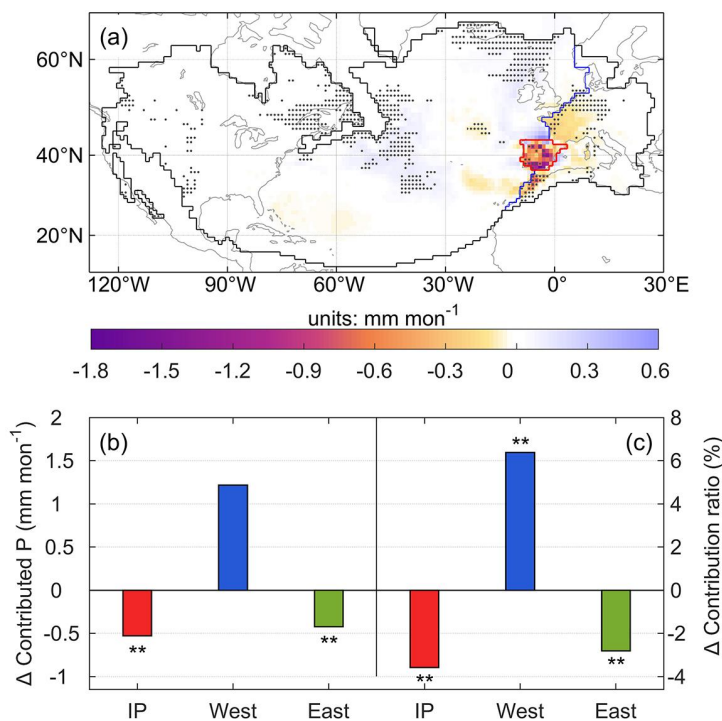
328

329 **Figure 7** (a) Difference in moisture contribution in the 90<sup>th</sup> precipitation shed between the dry years  
330 and the wet years (average of dry years minus average of wet years). The dots indicate 0.1  
331 significance of the difference. The changes in average precipitation contributed from each region  
332 (b) and their average contribution ratios (c) between the dry years and the wet years. ‘\*\*\*’ and ‘\*\*’  
333 represent 0.05 and 0.1 level significance of the difference.

334 The dry years in the two periods have been divided and compared with each other,  
335 and the differences between the two periods are shown in Fig. 8. From the distribution  
336 of differences, the grids with reduced moisture contribution are mainly located in the  
337 IP and the east region, and the southern part of the IP has the largest decrease (Fig. 8(a)).  
338 Mainly dominated by these negatively changing grids, both the absolute contribution



339 and the contribution ratio of the local IP and the east have dropped significantly, with  
 340 0.53 and 0.42 mm mon<sup>-1</sup> decrease in contributed precipitation and 3.58 % and 2.81 %  
 341 contribution ratio reduction, respectively (Fig. 8(b, c)). For the west region, however,  
 342 it raises the moisture contribution to the summer precipitation by 1.22 mm mon<sup>-1</sup> in dry  
 343 years after 1997, causing a 6.39 % increase in its contribution ratio. Despite the dry  
 344 years with no decrease precipitation between two periods, the decrease in local  
 345 recycling is still noticeable.



346  
 347 **Figure 8** (a) Difference in moisture contribution in the 90<sup>th</sup> precipitation shed in the dry years  
 348 between 1998-2019 and 1980-1997. The dots indicate 0.1 significance of the difference. The  
 349 changes in average precipitation contributed from each region (b) and their average contribution



350 ratios (c) in the dry years between 1998-2019 and 1980-1997. ‘\*\*\*’ and ‘\*\*’ represent 0.05 and 0.1  
351 level significance of the difference.

#### 352 **4. Discussion**

353 The trends in the contribution from the three source regions, the local, the west  
354 and the east regions, to all seasonal and annual precipitation over the past 40 years are  
355 listed in Table 1. In general, the decreasing trend maintained by the local IP and the east  
356 region are closely related to the drought in the Mediterranean basin (Ribeiro et al., 2020;  
357 Russo et al., 2019), and the increasing proportion of the west can be explained by the  
358 increasingly important role of the oceanic moisture in terrestrial precipitation (Gimeno  
359 et al., 2020; Vicente-Serrano et al., 2018). The simultaneous decrease in the moisture  
360 contribution from all three regions is responsible for the significant decrease in only the  
361 summer precipitation series among all seasonal or annual precipitation. In particular,  
362 the local recycling ratio in summer is obviously way down, differentiating the reduced  
363 summer precipitation from the other seasons. It is worth highlighting that this  
364 significant decrease in recent summer precipitation over the IP in this study is based on  
365 a short record (1980-2019) from ERA5, while a long-term assessment of precipitation  
366 (1850-2018) from multiple sources still lacks a statistically significant decreasing trend  
367 (Peña-Angulo et al., 2020). Nevertheless, the changes in the recent four decades still  
368 show the significant influence of the local recycling, especially on the trend of summer  
369 precipitation and variation of summer wet and dry years.

370



371 **Table 1** Trends of contributions from the IP, the west and the east to annual and seasonal  
372 precipitation, and the trends of their contribution ratios.

	Contributed precipitation (mm mon <sup>-1</sup> decade <sup>-1</sup> )					Contribution ratio (% decade <sup>-1</sup> )				
	Annual	Spring	Summer	Autumn	Winter	Annual	Spring	Summer	Autumn	Winter
IP	-0.24**	-0.30	-0.59**	-0.03	-0.03	-0.49**	-0.66**	-1.17**	-0.14	-0.08
West	0.53	1.67	-1.28*	1.23	0.52	0.81**	0.80	1.29**	0.38	0.77
East	-0.17	-0.06	-0.28	-0.05	-0.29	-0.32	-0.14	-0.12	-0.24	-0.69

373 \*\*\* and \*\* represent 0.05 and 0.1 level significance of the trend.

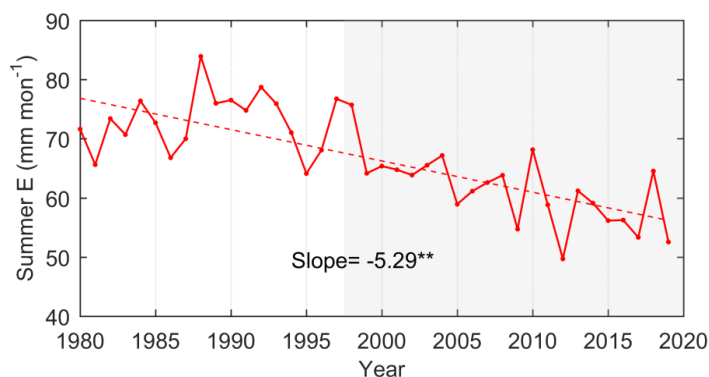
374 The remarkable decrement of summer precipitation can be attributed to the  
375 simultaneous and large reduction of contributions from all three source regions. The  
376 strong land-sea contrast caused by the warming land surface makes the advected air  
377 mass from Atlantic experience drying (Cramer et al., 2018; Kröner et al., 2017),  
378 resulting in a decrease in the moisture contribution from the Atlantic Ocean in the west  
379 to the IP precipitation. In addition, the extension of Hadley circulation makes the IP  
380 more strongly affected by subsidence with higher static stability and lower frequency  
381 of extreme heavy precipitation (Brogli et al., 2019). However, the ocean warming  
382 patterns and thermodynamics can promote precipitation in cold seasons (Brogli et al.,  
383 2019), just as shown by the increasing contributed precipitation from the west in  
384 autumn and winter in Table 1. It suggests the drivers leading to less summer  
385 precipitation do not generally cause a similar change in precipitation in the other  
386 seasons.

387 As an important indicator to describe the interaction between the surface and





388 atmospheric processes, the change in precipitation recycling ratio takes into account  
389 changes in both precipitation and the contribution of local evaporation (Goessling and  
390 Reick, 2011). For the IP, its significant reduction in local moisture contribution is most  
391 likely due to the weakening of local evaporation (Fig. 9). Due to the positive correlation  
392 between soil moisture and precipitation in summer, the declining precipitation leads to  
393 the shortage of soil water supply, the limitation of soil water evaporation capacity and  
394 the consequent reduction in surface evaporation (García-Valdecasas Ojeda et al., 2020;  
395 Ruosteenoja et al., 2018). Especially in summer, when the soil moisture and recycling  
396 process driven by evaporation are regarded as an active source of moisture (Jung et al.,  
397 2010; Vicente-Serrano et al., 2014) , this weakening of the local moisture recycling  
398 again leads to a decrease in precipitation. This continuous feedback of the interactions  
399 of soil moisture evaporation and precipitation can exacerbate the water resource  
400 depletion and summer drought.



401

402 **Figure 9** Time series of IP summer evaporation from ERA5 during 1980-2019 (unit of the slope:

403  $\text{mm mon}^{-1} \text{ decade}^{-1}$ ). \*\*\* represents 0.05 level significance of the trend.



## 404 **5. Conclusions**

405 In this study, using the reanalysis data ERA5 and WAM-2layers model, we  
406 investigated how changes in moisture contribution from the source affect the reduction  
407 in summer precipitation between 1980-1997 and 1998-2019. The major findings are  
408 summarized below.

409 1) The reduction of contribution to IP summer precipitation is mainly concentrated in  
410 the IP and its neighboring grids. The local IP grids show the greatest reduction, and  
411 the surrounding grids show a slight but significant decrease.

412 2) Compared with the period of 1980-1997, the decrease in the moisture contribution  
413 from the IP, the west and the east during 1998-2019 results in the reductions of 1.7,  
414 3.6, and 1.1 mm mon<sup>-1</sup> of the IP precipitation, accounting for 26 %, 57 %, and 17 %  
415 of the main source supply reduction, respectively.

416 3) The contributions from the local IP and the east keep declining during the 40 years.  
417 In particular, the significant reduction in local recycling, reflected in the  
418 disappearance of wet years after 1997 and the reduction of local contributions in  
419 dry years, suggests a close link with the decrease in summer precipitation.

420

### 421 **Code and Data availability**

422 Code and data used in this manuscript are available from the corresponding author upon  
423 a reasonable request.

424



425 **Author contributions**

426 MG and QT designed the study; YL performed the analysis and calculation; CZ  
427 contributed to the application of the model in this study; YL prepared the manuscript  
428 draft, and all co-authors reviewed and edited the manuscript.

429

430 **Competing interests**

431 The authors declare no competing interests.

432

433 **Acknowledgements**

434 This study was partly funded by the National Natural Science Foundation of China  
435 (41730645) and the Strategic Priority Research Program of Chinese Academy of  
436 Sciences (XDA20060402). The authors would like to thank the EU and Innovation  
437 Fund Denmark (IFD) for funding within the framework of the FORWARD  
438 collaborative international consortium financed through the ERA-NET co-fund  
439 WaterWorks2015 integral part of the 2016 joint activities developed by the “Water  
440 Challenges for a Changing World” joint programme initiative (Water JPI).

441



## 442 References

- 443 Boé, J., and Terray, L.: Land–sea contrast, soil-atmosphere and cloud-temperature  
444 interactions: interplays and roles in future summer European climate change,  
445 *Clim. Dyn.*, 42, 683-699, <https://doi.org/10.1007/s00382-013-1868-8>, 2014.
- 446 Boé, J., Terray, L., Cassou, C., and Najac, J.: Uncertainties in European summer  
447 precipitation changes: role of large scale circulation, *Clim. Dyn.*, 33, 265-276,  
448 <https://doi.org/10.1007/s00382-008-0474-7>, 2009.
- 449 Bonne, J. L., Masson-Delmotte, V., Cattani, O., Delmotte, M., and Steen-Larsen, H. C.:  
450 The isotopic composition of water vapour and precipitation in Ivittuut, Southern  
451 Greenland, *Atmos. Chem. Phys.*, 14, 4419-2014, <https://doi.org/10.5194/acp-14-4419-2014>, 2014.
- 453 Brogli, R., Sørland, S. L., Kröner, N., and Schär, C.: Causes of future Mediterranean  
454 precipitation decline depend on the season, *Environ. Res. Lett.*, 14, 114017,  
455 <https://doi.org/10.1088/1748-9326/ab4438>, 2019.
- 456 Burde, G. I.: Bulk recycling models with incomplete vertical mixing. Part I: Conceptual  
457 framework and models, *J. Clim.*, 19, 1461-1472,  
458 <https://doi.org/10.1175/jcli3687.1>, 2010.
- 459 Cortesi, N., Trigo, R. M., Gonzalez-Hidalgo, J. C., and Ramos, A. M.: Modeling  
460 monthly precipitation with circulation weather types for a dense network of  
461 stations over Iberia, *Hydrol. Earth Syst. Sci.*, 17, 665-678,  
462 <https://doi.org/10.5194/hess-17-665-2013>, 2013.
- 463 Cramer, W., Guiot, J., Fader, M., Garrabou, J., Gattuso, J.-P., Iglesias, A., . . . Xoplaki,  
464 E.: Climate change and interconnected risks to sustainable development in the  
465 Mediterranean, *Nat. Clim. Chang.*, 8, 972-980, <https://doi.org/10.1038/s41558-018-0299-2>, 2018.
- 467 Damián, I.-C., and Gonzalo, M. M.: A new moisture tagging capability in the Weather  
468 Research and Forecasting model: formulation, validation and application to the  
469 2014 Great Lake-effect snowstorm, *Earth Syst. Dynam.*, 9, 167-185,  
470 <https://doi.org/10.5194/esd-9-167-2018>, 2018.
- 471 García-Valdecasas Ojeda, M., Yeste, P., Gámiz-Fortis, S. R., Castro-Díez, Y., and  
472 Esteban-Parra, M. J.: Future changes in land and atmospheric variables: An  
473 analysis of their couplings in the Iberian Peninsula, *Sci. Total Environ.*, 722,  
474 137902, <https://doi.org/10.1016/j.scitotenv.2020.137902>, 2020.
- 475 Gimeno, L., Nieto, R., and Sorí, R.: The growing importance of oceanic moisture  
476 sources for continental precipitation, *npj Clim. Atmos. Sci.*, 3, 27,  
477 <https://doi.org/10.1038/s41612-020-00133-y>, 2020.
- 478 Gimeno, L., Nieto, R., Trigo, R. M., Vicente-Serrano, S. M., and López-Moreno, J. I.:  
479 Where does the Iberian Peninsula moisture come from? An answer based on a  
480 Lagrangian approach, *J. Hydrometeorol.*, 11, 421-436,  
481 <https://doi.org/10.1175/2009JHM1182.1>, 2010.



- 482 Goessling, H. F., and Reick, C. H.: What do moisture recycling estimates tell us?  
483 Exploring the extreme case of non-evaporating continents, *Hydrol. Earth Syst.*  
484 *Sci.*, 15, 3217-3235, <https://doi.org/10.5194/hess-15-3217-2011>, 2011.
- 485 Goessling, H. F., and Reick, C. H.: On the "well-mixed" assumption and numerical 2-  
486 D tracing of atmospheric moisture, *Atmos. Chem. Phys.*, 13, 5567-5585,  
487 <https://doi.org/10.5194/acp-13-5567-2013>, 2013.
- 488 Herrera, S., Cardoso, R. M., Soares, P. M., Espírito-Santo, F., and Gutiérrez, J.: Iberia01:  
489 a new gridded dataset of daily precipitation and temperatures over Iberia, *Earth*  
490 *Syst. Sci. Data*, 11, 1947-1956, <https://doi.org/10.5194/essd-11-1947-2019>,  
491 2019.
- 492 Hersbach, H., Bell, B., Berrisford, P., Hirahara, S., Horányi, A., Muñoz-Sabater, J., . . .  
493 Thépaut, J.-N.: The ERA5 global reanalysis, *Quarterly Journal of the Royal*  
494 *Meteorological Society*, 146, 1999-2049, <https://doi.org/10.1002/qj.3803>, 2020.
- 495 Jung, M., Reichstein, M., Ciais, P., Seneviratne, S. I., Sheffield, J., Goulden, M. L., . . .  
496 Zhang, K.: Recent decline in the global land evapotranspiration trend due to  
497 limited moisture supply, *Nature*, 467, 951-954,  
498 <https://doi.org/10.1038/nature09396>, 2010.
- 499 Keys, P. W., Gordon, L. J., . . . R.: Variability of moisture recycling using a  
500 precipitationshed framework, *Hydrol. Earth Syst. Sci.*, 18, 3937-3950,  
501 <https://doi.org/10.5194/hess-18-3937-2014>, 2014.
- 502 Keys, P. W., Ent, R., Gordon, L. J., Hoff, H., and Savenije, H.: Analyzing  
503 precipitationsheds to understand the vulnerability of rainfall dependent regions,  
504 *Biogeosciences*, 8, 733-746, <https://doi.org/10.5194/bg-9-733-2012>, 2011.
- 505 Kröner, N., Kotlarski, S., Fischer, E., Lüthi, D., Zubler, E., and Schär, C.: Separating  
506 climate change signals into thermodynamic, lapse-rate and circulation effects:  
507 theory and application to the European summer climate, *Clim. Dyn.*, 48, 3425-  
508 3440, <https://doi.org/10.1007/s00382-016-3276-3>, 2017.
- 509 Lenderink, G., van Ulden, A., van den Hurk, B., and van Meijgaard, E.: Summertime  
510 inter-annual temperature variability in an ensemble of regional model  
511 simulations: analysis of the surface energy budget, *Clim. Change*, 81, 233-247,  
512 <https://doi.org/10.1007/s10584-006-9229-9>, 2007.
- 513 Lopez-Bustins, J. A., and Lemus-Canovas, M.: The influence of the Western  
514 Mediterranean Oscillation upon the spatio-temporal variability of precipitation  
515 over Catalonia (northeastern of the Iberian Peninsula), *Atmos. Res.*, 236,  
516 104819, <https://doi.org/10.1016/j.atmosres.2019.104819>, 2020.
- 517 Numaguti, A.: Origin and recycling processes of precipitating water over the Eurasian  
518 continent: Experiments using an atmospheric general circulation model, *J.*  
519 *Geophys. Res.-Atmos.*, 104, 1957-1972,  
520 <https://doi.org/10.1029/1998JD200026>, 1999.
- 521 Páscoa, P., Russo, A., Gouveia, C. M., Soares, P. M. M., Cardoso, R. M., Careto, J. A.  
522 M., and Ribeiro, A. F. S.: A high-resolution view of the recent drought trends



- 523 over the Iberian Peninsula, *Weather Clim. Extremes*, 32, 100320,  
524 <https://doi.org/10.1016/j.wace.2021.100320>, 2021.
- 525 Peña-Angulo, D., Vicente-Serrano, S. M., Domínguez-Castro, F., Murphy, C., Reig, F.,  
526 Trambly, Y., . . . El Kenawy, A.: Long-term precipitation in Southwestern  
527 Europe reveals no clear trend attributable to anthropogenic forcing, *Environ.*  
528 *Res. Lett.*, 15, 094070, <https://doi.org/10.1088/1748-9326/ab9c4f>, 2020.
- 529 Rajczak, J., and Schär, C.: Projections of future precipitation extremes over Europe: A  
530 multimodel assessment of climate simulations, *J. Geophys. Res.-Atmos.*, 122,  
531 10,773-710,800, <https://doi.org/10.1002/2017JD027176>, 2017.
- 532 Ribeiro, A. F. S., Russo, A., Gouveia, C. M., and Pires, C. A. L.: Drought-related hot  
533 summers: A joint probability analysis in the Iberian Peninsula, *Weather Clim.*  
534 *Extremes*, 30, 100279, <https://doi.org/10.1016/j.wace.2020.100279>, 2020.
- 535 Ruosteenoja, K., Markkanen, T., Venäläinen, A., Räisänen, P., and Peltola, H.: Seasonal  
536 soil moisture and drought occurrence in Europe in CMIP5 projections for the  
537 21st century, *Clim. Dyn.*, 50, 1177-1192, [https://doi.org/10.1007/s00382-017-](https://doi.org/10.1007/s00382-017-3671-4)  
538 [3671-4](https://doi.org/10.1007/s00382-017-3671-4), 2018.
- 539 Russo, A., Gouveia, C. M., Dutra, E., Soares, P. M. M., and Trigo, R. M.: The synergy  
540 between drought and extremely hot summers in the Mediterranean, *Environ.*  
541 *Res. Lett.*, 14, 014011, <https://doi.org/10.1088/1748-9326/aaf09e>, 2019.
- 542 Serrano, A., García, J. A., Mateos, V. L., Cencillo, M. L., and Garrido, J.: Monthly  
543 modes of variation of precipitation over the Iberian Peninsula, *J. Clim.*, 12,  
544 2894-2919, 1999.
- 545 Stohl, A., and James, P.: A Lagrangian analysis of the atmospheric branch of the global  
546 water cycle. Part I: Method description, validation, and demonstration for the  
547 August 2002 flooding in Central Europe, *J. Hydrometeorol.*, 5, 656, 2004.
- 548 Stohl, A., and James, P.: A Lagrangian analysis of the atmospheric branch of the global  
549 water cycle. Part II: Moisture transports between earth's ocean basins and river  
550 catchments, *J. Hydrometeorol.*, 6, 961-984, <https://doi.org/10.1175/JHM470.1>,  
551 2005.
- 552 Tang, Q., Leng, G., and Groisman, P. Y.: European hot summers associated with a  
553 reduction of cloudiness, *J. Clim.*, 25, 3637-3644, [https://doi.org/10.1175/JCLI-](https://doi.org/10.1175/JCLI-D-12-00040.1)  
554 [D-12-00040.1](https://doi.org/10.1175/JCLI-D-12-00040.1), 2012.
- 555 Teuling, A. J., Van Loon, A. F., Seneviratne, S. I., Lehner, I., Aubinet, M., Heinesch,  
556 B., . . . Spank, U.: Evapotranspiration amplifies European summer drought,  
557 *Geophys. Res. Lett.*, 40, 2071-2075, <https://doi.org/10.1002/grl.50495>, 2013.
- 558 Ulbrich, U., Christoph, M., Pinto, J. G., and Corte-Real, J.: Dependence of winter  
559 precipitation over Portugal on NAO and baroclinic wave activity, *International*  
560 *Journal of Climatology*, 19, 379-390, [https://doi.org/10.1002/\(SICI\)1097-](https://doi.org/10.1002/(SICI)1097-0088(19990330)19:4<379::AID-JOC357>3.0.CO;2-8)  
561 [0088\(19990330\)19:4<379::AID-JOC357>3.0.CO;2-8](https://doi.org/10.1002/(SICI)1097-0088(19990330)19:4<379::AID-JOC357>3.0.CO;2-8), 2015.
- 562 van der Ent, R. J., and Savenije, H. H. G.: Length and time scales of atmospheric  
563 moisture recycling, *Atmos. Chem. Phys.*, 11, 1853-1863,



- 564 <https://doi.org/10.5194/acp-11-1853-2011>, 2011.
- 565 van der Ent, R. J., Savenije, H. H. G., Schaeffli, B., and Steele-Dunne, S. C.: Origin and  
566 fate of atmospheric moisture over continents, *Water Resour. Res.*, 46,  
567 <https://doi.org/10.1029/2010WR009127>, 2010.
- 568 van der Ent, R. J., Tuinenburg, O. A., Knoche, H. R., Kunstmann, H., and Savenije, H.  
569 H. G.: Should we use a simple or complex model for moisture recycling and  
570 atmospheric moisture tracking?, *Hydrol. Earth Syst. Sci.*, 17, 4869-4884,  
571 <https://doi.org/10.5194/hess-17-4869-2013>, 2013.
- 572 van der Ent, R. J., Wang-Erlandsson, L., Keys, P., and Savenije, H.: Contrasting roles  
573 of interception and transpiration in the hydrological cycle - Part 2: Moisture  
574 recycling, *Earth Syst. Dynam.*, 5, <https://doi.org/10.5194/esdd-5-281-2014>,  
575 2014.
- 576 Vicente-Serrano, S. M., Azorin-Molina, C., Sanchez-Lorenzo, A., Morán-Tejeda, E.,  
577 Lorenzo-Lacruz, J., Revuelto, J., . . . Espejo, F.: Temporal evolution of surface  
578 humidity in Spain: recent trends and possible physical mechanisms, *Clim. Dyn.*,  
579 42, 2655-2674, <https://doi.org/10.1007/s00382-013-1885-7>, 2014.
- 580 Vicente-Serrano, S. M., Nieto, R., Gimeno, L., Azorin-Molina, C., Drumond, A., El  
581 Kenawy, A., . . . Peña-Gallardo, M.: Recent changes of relative humidity:  
582 regional connections with land and ocean processes, *Earth Syst. Dynam.*, 9,  
583 915-937, <https://doi.org/10.5194/esd-9-915-2018>, 2018.
- 584 Zhu, Y., and Newell, R. E.: A proposed algorithm for moisture fluxes from atmospheric  
585 rivers, *Mon. Weather Rev.*, 126, 725-735, [https://doi.org/10.1175/1520-  
586 0493\(1998\)126<0725:Apafmf>2.0.Co;2](https://doi.org/10.1175/1520-0493(1998)126<0725:Apafmf>2.0.Co;2), 1998.
- 587